Nanomechanics of Twisted Mono- and Few-Layer Graphene Nanoribbons

ARTICLE *in* JOURNAL OF PHYSICAL CHEMISTRY LETTERS · MAY 2013

Impact Factor: 7.46 · DOI: 10.1021/jz400747f

2 AUTHORS, INCLUDING:

Traian Dumitrică
University of Minnesota Twin Cities
92 PUBLICATIONS **1,428** CITATIONS

THE JOURNAL OF PHYSICAL CHEMISTRY Letters

Letter

pubs.acs.org/JPCL

Nanomechanics of Twisted Mono- and Few-Layer Graphene Nanoribbons

Evgeniya Dontsova and Traian Dumitrică*

Department of Mechanical Engineering, University of Minnesota, Minneapolis, Minnesota 55455, United States

ABSTRACT: Enabled by the technique of objective molecular dynamics, we reveal the unusual mechanics exhibited by nanoscale twisted graphene nanoribbons containing up to seven layers. Unlike in a linear-elastic plate, we find that the deformation practically does not contain contributions associated with in-plane shearing but largely with inhomogeneous stretching and compression of the constituent layers. The whole twisted structure undergoes shortening when no axial force is applied, while the constituent layers store various strain energies, depending on their location. We capture this behavior with a simple model and show that the deviations from the plate model are increasing with the number of layers and width of the ribbon. Our results are especially relevant for the experimental efforts of measuring graphene's shear modulus.

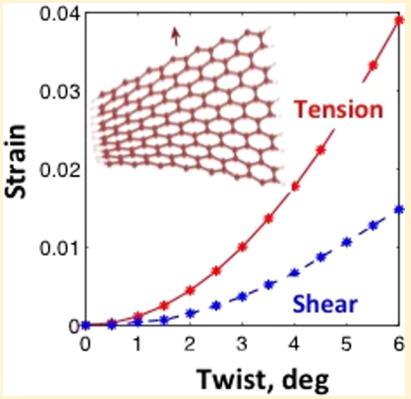

SECTION: Physical Processes in Nanomaterials and Nanostructures

Due to the current drive toward miniaturization, understanding and modeling the mechanics of nanostructures become of prime importance.[1−3] In carbon materials, the interest has shifted over the past decade from carbon nanotubes[4,5] to graphene,[6] now viewed as the quintessential nanomaterial. Understanding the fundamental deformation modes of graphene becomes even more important due to the recent interest in developing graphene-based composite materials.[7,8] Advanced characterization experiments[9−14] were carried out to measure the elastic constants of the mono- and few-layer-thick graphene, such as Young's modulus (1 TPa assuming a 3.35 Å monolayer thickness)[10] and bending rigidity of bilayer graphene (∼35 eV).[11] Shear moduli for multilayers (53 GPa) and even monolayers (280 GPa)[13,14] were reported from experiments in which twist graphene structures clung onto a mechanical double-paddle oscillator.

On the theoretical site, the in-plane elastic and flexural properties have been relatively well explored particularly through microscopic simulations.[15−19] The out-of-plane deformations are more subtle due to the atomic-scale thickness of these structures. Recently, we revealed the breakdown of the plate phenomenology in the pure bending and wrinkling of graphene.[20,21] Interestingly, the bent multilayer can still exhibit plate mechanics, especially in experiments in which the load is applied directly on the free ends of the nanostructure.[22] Unfortunately, the validity of the plate behavior often invoked (see, for example, refs 13 and 14) in relation to the twist deformation of mono- and few-layer-thick graphene has not been yet examined.

Simulating a continuous twisting deformation at the atomic scale cannot be performed with standard theoretical approaches. Thus, an investigation of the purported connection between the nanomechanics and the elastic plate mechanics calls for a special approach. Indeed, twisted structures with a uniform helical symmetry have a unit cell size corresponding to the size of the helical motif. Such a large number of atoms prohibits ab initio calculations adopting translational symmetry via periodic boundary conditions. Instead, here, we use objective boundary conditions[23,24] and ab initio parametrized density functional[25,26] description of bonding cured to describe the interlayer van der Waals interactions.[27] The simplifications in the number of atoms introduced by this methodology were successfully exploited before for example to understand the torsional response of twisted carbon nanotubes.[28,29]

In our investigation method, titled objective molecular dynamics (MD),[23] an infinitely long graphene nanoribbon (GNR) twisted at an arbitrary θ/T rate is described with the objective structure formula[30]

$$\mathbf{X}_{j,\zeta} = \mathbf{R}^{\zeta}\mathbf{X}_j + \zeta\mathbf{T} \qquad -\infty < \zeta < \infty \tag{1}$$

Index j runs over the atomic positions $\mathbf{X}_j$ located in the primitive cell, and $\mathbf{R}$ is a rotational matrix of angle θ around the axis parallel with vector $\mathbf{T}$ of modulus T. We study the torsional behavior of a collection of multilayered GNRs with H-saturated armchair edges and a number of layers N_l = 1, ..., 7 stacked in an alternative AB manner. The number of dimer lines in each layer is N_d = 14. Thus, the objective MD calculations were carried on $28N_l$ carbon and $4N_l$ edge hydrogen atoms, regardless of the twist rate. We first relax the flat structures

Received: April 8, 2013
Accepted: May 30, 2013
Published: May 30, 2013

to find the optimal T. The twist calculations involve two stages. We relax the atomic positions under twist angle θ at constant T. Next, we relax the twisted GNR under parameter T at the considered θ. The ability of this method to describe torsional deformations is demonstrated in Figure 1, showing three

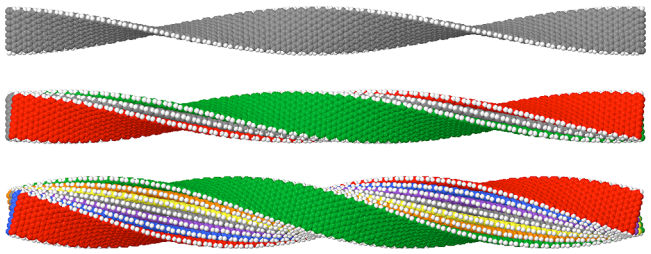

Figure 1. Objective MD simulations of 14 °/nm twisted mono-, three-, and seven-layer N_d = 14 GNRs (top to bottom).

example calculations comprising relaxed GNRs under the boundary conditions of eq 1. In all of these morphologies, vector **T** is located on the central (gray) layer axis, which remains straight under twist. The axes of all other layers turn into helices.

In linear plate mechanics, the strain energy caused by twisting has two components, the in-plane shear strain energy introduced by warping E_w and the out-of-plane strain energy.[31] E_w should dominate in the transverse isotropic graphene material. In a sandwich of plates model, each with thickness Z_0 = 3.35 Å, the in-plane shear strain under a twist rate θ/T increases with the distance from the twist axis to the layer n, $h_n = Z_0(n - (N_l + 1)/2)$, as

$$\gamma_n = \frac{h_n\theta}{T} \tag{2}$$

Thus, E_w (eV per atom) is written

$$E_w = \frac{1}{N_l}\sum_{n=1}^{N_l}\frac{G\gamma_n^2}{2} = G\frac{Z_0^2N_l^2}{24T^2}\left[1 - \frac{1}{N_l^2}\right]\theta^2 \tag{3}$$

where G is the in-plane shear modulus of graphene. Large shears should lead to the creation of normal elongation strains, a behavior known as the Poynting effect.[32]

While plate mechanics response is a reasonable hypothesis,[14] the features described above are not present in the microscopic data shown in Figure 2. Indeed, (i) E_w predicted with eq 3 and G = 25.3 eV[28] grossly overestimates the computed total strain energy of a seven-layer GNR, Figure 2a. Moreover, (ii) the profile of the strain energy distribution per layer is different from the plate behavior expectations, Figure 2b. Even more, (iii) the microscopic measurement of the averaged shear strain stored in each layer is negligible at all considered twist levels,[33] Figure 2c, in disagreement with eq 2. For better clarity, in Figure 2d, we illustrate the microscopic twist deformation for the three-layer GNR. The top view reveals that the noncentral layers are simply rotated relative to the central one, without storing shear. For a comparison, Figure 2d, right displays a sheared multilayered structure. Finally, (iv) we also noted that GNRs tend to compress under twisting, a behavior we refer to as the "reverse-Poynting" effect. Table 1 gives the magnitude of

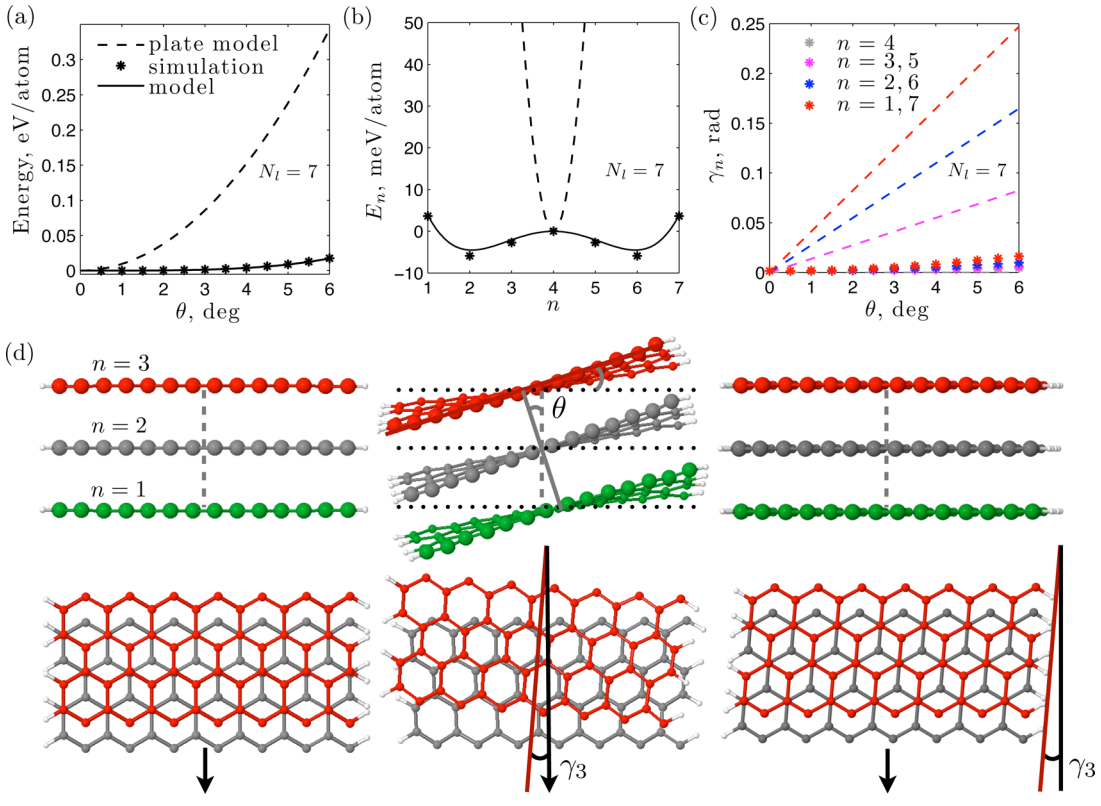

Figure 2. Comparison between the atomistic simulation results (symbols), plate model (dashed line), and constructed model given by eq 5 (solid line) predictions for seven-layer GNR of (a) strain energy (at $\varepsilon = 0$), (b) energy per layer versus the layer number (at $\varepsilon = \varepsilon^{Py}$), and (c) shear strain as functions of the twist angle. (d) The axial and top views on the undistorted (left), twisted by 14 °/nm (central), and sheared (right) three-layer N_d = 14 GNRs configurations, where arrows denote the twist axis. Note that only two upper layers are shown in the top view.

dx.doi.org/10.1021/jz400747f | J. Phys. Chem. Lett. 2013, 4, 2010−2014

Table 1. Reverse-Poynting Strains for 14 °/nm Twisted GNRs with a Different Number of Layers N_l

N_l	1	2	3	4	5	6	7
ε^{Py}, %	−0.54	−0.68	−0.80	−1.04	−1.33	−1.65	−1.91

the reverse Poynting strain ε^{Py}, showing an increase with the number of layers.

The departure (i−iv) from the expected classical plate mechanics poses the natural question, What is the main source of strain in the torsionally deformed GNRs? To understand it, Figure 3 details the interlayer deformation along the dimer lines

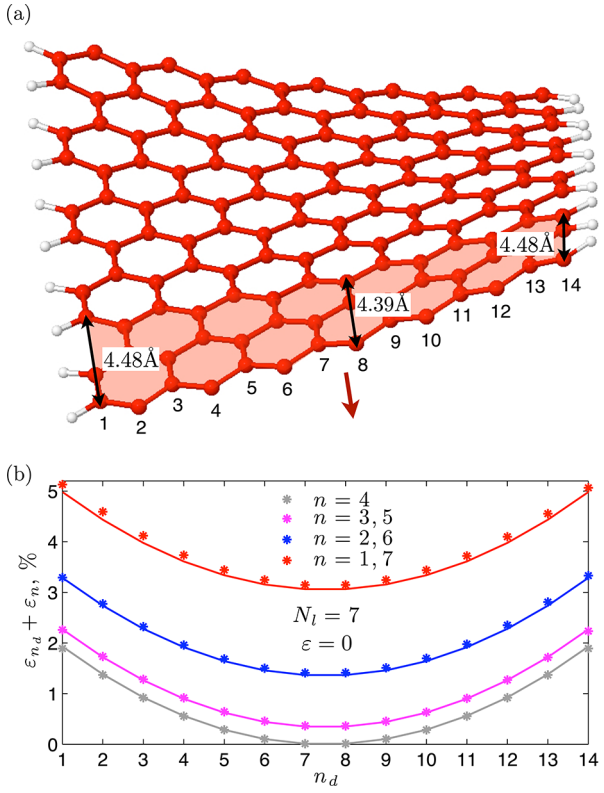

Figure 3. (a) Atomistic representation of the uppermost $n = 1$ layer of the seven-layer $N_d = 14$ GNR, where the arrow denotes this layer axis and (b) plot of the local tensile strains versus the dimer number for different layers of the seven-layer GNR at a 14 °/nm twist and $\varepsilon = 0$. Simulation results are denoted by symbols, and model predictions are shown by solid lines.

in a simulation considering $\theta = 6°$ while T is kept at the initial value of 4.26 Å corresponding to the stress-free flat GNR (i.e., $\varepsilon = 0$, first stage of twisting). We note that unlike in the flat case, the distance between corresponding atoms in neighboring replicas of the simulated cell varies along the GNR's width. Thus, the distribution of tensional strain stored in twisted GNRs is inhomogeneous, with the outermost dimer lines being most stretched, Figure 3a. Figure 3b demonstrates that this inhomogeneity is qualitatively similar in all layers. (Yet, the twisted multilayered GNR can be described with one axial length T.) It is useful to quantify the tensile strain in each layer with the effective strain quantity ε_n^{eff}, defined as an average tensile strain in a monolayer.[34] This is because the electronic band gap attributes depend directly[34] on ε_n^{eff}. Using simple geometric considerations, we obtained

$$\varepsilon_n^{eff} = \theta^2\left[\frac{(N_d^2 - 1)a_{C-C}^2}{32T^2} + \frac{h_n^2}{2T^2}\right] \quad (4)$$

where $a_{C-C} = 1.42$ Å is the length of the C−C bond. This expression is in excellent agreement with measured microscopic data, Figure 4a, and indicates that the constituent twisted layers

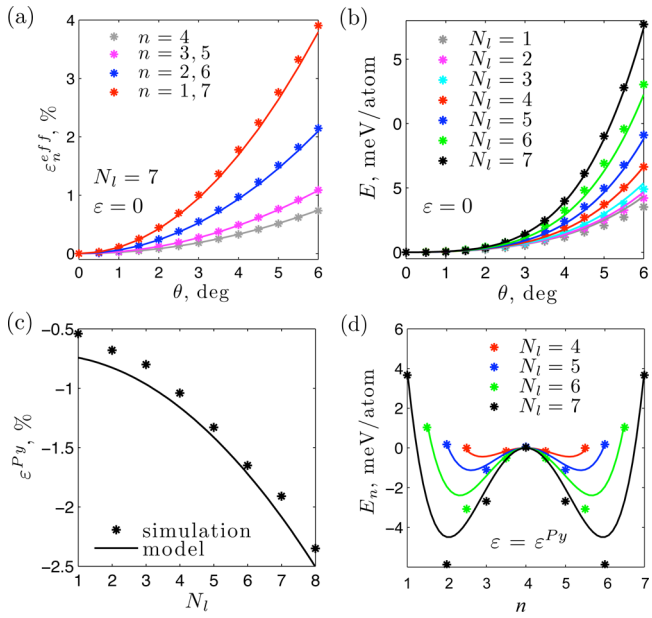

Figure 4. (a) Graph of the effective tensile strain as a function of the twist angle for different layers of seven-layer $N_d = 14$ GNR and (b) plot of the strain energy versus the twist angle for GNRs with different number of layers N_l. Comparisons between the simulation results and model predictions for (c) the reverse-Poynting strain plotted as a function of the number of layers and (d) the energy per layer E_n versus the layer position in the twisted by 14 °/nm multilayer GNRs. Here, simulation results are shown by symbols, while model predictions are represented by solid lines.

will have different band gap values under twisting. For example, in $N_l = 7$ GNR under 14 °/nm, we measured $\varepsilon_7^{eff} = 3.9\%$ with a band gap of 0.41 eV, while $\varepsilon_4^{eff} = 0.73\%$ with a band gap of only 0.03 eV.

For an extensive characterization of twisted GNRs, we build a simple model grounded on symmetry considerations and the discrete summation of the stretching strains along all dimer lines. We write the strain energy E of a twisted−axially strained GNR as a polynomial functional in θ

$$E = E_0(\varepsilon) + E_2(\varepsilon)\theta^2 + E_4\theta^4 \quad (5)$$

Here, ε denotes the axial strain in the GNR measured with respect to the relaxed flat structure. There are no odd powers in θ terms because left- and right-handed twisting are energetically equivalent. The coefficients E_0, E_2, and E_4 are identified using microscopic considerations, as follows. This strain energy E contains (first stage of twisting) a stretching component

dx.doi.org/10.1021/jz400747f | J. Phys. Chem. Lett. 2013, 4, 2010−2014

$$E_s = \frac{C}{2N_dN_l}\sum_{n=1}^{N_l}\sum_{n_d=1}^{N_d}(\varepsilon + \varepsilon_{n_d} + \varepsilon_n)^2 \quad (6)$$

and a small contribution associated with the twist-induced misalignment of the π-orbitals[35]

$$E_\pi = \alpha\theta^2 \quad (7)$$

Here, $\varepsilon_{n_d} = d_{n_d}^2\theta^2/2T^2$ is the axial strain at dimer line n_d located $d_{n_d} = (3^{1/2}a_{C-C}/2)(n_d - (N_d + 1)/2)$ distance apart from the central line of a layer, $\varepsilon_n = h_n^2\theta^2/2T^2$ is the axial strain caused by twist on layer n, C is the in-plane stiffness, and α is the nearest-neighbor hopping parameter for aligned π-orbitals. After some algebra, we obtained

$$E_0 = \frac{C\varepsilon^2}{2} \quad (8)$$

$$E_2 = \alpha + \left[\frac{C(N_d^2 - 1)a_{C-C}^2}{32T^2} + \frac{C(N_l^2 - 1)}{24}\frac{Z_0^2}{T^2}\right]\varepsilon \quad (9)$$

$$E_4 = \left[\frac{C(3N_d^2 - 7)(N_d^2 - 1)}{135\cdot 2^{11}} + \frac{C(N_d^2 - 1)(N_l^2 - 1)}{27\cdot 2^8}\frac{Z_0^2}{T^2} + \frac{C(3N_l^2 - 7)(N_l^2 - 1)}{15\cdot 2^7}\frac{Z_0^4}{T^4}\right] \quad (10)$$

Thus, E_0, E_2, and E_4 have clear significances; eq 8 accounts for tensile or compressive deformations, eq 9 includes the effects of π-orbital misalignment[35] and layers stretching, while eq 10 comprises the stretching energy that comes from twisting. Figure 4b shows that energies computed by objective MD can be already well predicted by the model eq 5 with parameters C = 50 eV (found from separate stretching calculations on N_d = 14 GNR) and α = 0.172 eV (taken from fitting of the total strain energy given by simulations to eq 5 for monolayer GNRs) for the whole collection of twisted GNRs with ε = 0.

The unusual twisting mechanics observed in the microscopic calculations is fully captured by this model. For example, ε^{Py} can be predicted by minimizing eq 5 with respect to ε at constant θ (second stage of twisting). This gives

$$\varepsilon^{Py} = -\theta^2\left[\frac{(N_d^2 - 1)a_{C-C}^2}{32T^2} + \frac{(N_l^2 - 1)}{24}\frac{Z_0^2}{T^2}\right] \quad (11)$$

Figure 4c demonstrates good agreement between the simulation results and predictions of eq 11, clearly showing the increase in $|\varepsilon^{Py}|$ with N_l. Equation 11 also predicts that the effect increases with the GNR's width (measured by N_d). Moreover, a comparison of eq 11 with the effective strain expression eq 4 gives $\varepsilon^{Py} = -(1/N_l)\sum_{n=1}^{N_l}\varepsilon_n^{eff}$, that is, the compression relieves the total effective strain created by varying θ. Thus, the reverse-Poynting effect originates in the relaxation of the accumulated effective tensile strain. This is distinct from the classical Poynting effect, a nonlinear elastic effect responding to an imposed shear.[32] The distribution of strain energy per layer depends on the interplay between the inhomogeneous layer stretching and reverse-Poynting compression. As exemplified in Figure 4d, this model also captures well the unexpected strain energy distribution among layers. Interestingly, the energy profile depends not only on θ but also on N_l; the outermost layers are much more strained than the inner ones and therefore more likely to fracture in combined torsion-elongation tests.

In conclusion, simulations of the torsional response of few-layer-thick GNRs have been so far hindered by the incompatibility of this fundamental deformation mode with the standard periodic boundary conditions. Enabled by the technique of objective MD coupled to an ab initio parametrized description of bonding, we provide a detailed microscopic view into this complex torsional mechanics. The results of our comprehensive simulations were captured very well by a simple phenomenological model that describes the reverse-Poynting effect and strain energy distribution among layers. This model does not contain any in-plane shear strain and can be also used to predict, without the need for further calculations, the torsional response of wider and thicker few-layer GNRs.

From the experimental response to torsional deformations[14] and assuming the linear-elastic plate phenomenology, a 280 GPa in-plane shear constant value was attributed to graphene. Here, we find that this classical plate model is unable to describe the torsional deformation in both mono- and few-layer unsupported GNRs. In fact, because the constituent graphene layers twist practically without shearing (the response is dominated by terms eqs 9 and 10), we uncover additional difficulties in connecting such experimental measurements with the graphene's in-plane shearing constant.

AUTHOR INFORMATION

Corresponding Author

*E-mail: dtraian@me.umn.edu.

Notes

The authors declare no competing financial interest.

ACKNOWLEDGMENTS

We thank I. Nikiforov for help with the Trocadero code. This work was supported by the NSF CAREER Grant CMMI-0747684. Computations were carried out at the Minnesota Supercomputing Institute.

REFERENCES

(1) Bhattacharya, K.; James, R. D. A Theory of Thin Films of Martensitic Materials with Applications to Microactuators. *J. Mech. Phys. Solids* **1999**, *47*, 531−576.

(2) Friesecke, G.; James, R. D. A Scheme for the Passage from Atomic to Continuum Theory for Thin Films, Nanotubes and Nanorods. *J. Mech. Phys. Solids* **2000**, *48*, 1519−1540.

(3) Friesecke, G.; Mueller, S.; James, R. D. A Hierarchy of Plates Models Derived from Nonlinear Elasticity by Γ-Convergence. *Arch. Ration. Mech. Anal.* **2006**, *180*, 183−236.

(4) Yu, M.-F.; Lourie, O.; Dyer, M. J.; Moloni, K.; Kelly, T. F.; Ruoff, R. S. Strength and Breaking Mechanism of Multiwalled Carbon Nanotubes under Tensile Load. *Science* **2000**, *287*, 637−640.

(5) Dumitrică, T.; Hua, M.; Yakobson, B. I. Symmetry, Time, and Temperature Dependent Strength of Carbon Nanotubes. *Proc. Natl. Acad. Sci. U.S.A.* **2006**, *103*, 6105−6109.

(6) Novoselov, K. S.; Geim, A. K.; Morozov, S. V.; Jiang, D.; Zhang, Y.; Dubonos, S. V.; Grigorieva, I. V.; Firsov, A. A. Electric Field Effect in Atomically Thin Carbon Films. *Science* **2004**, *306*, 666−669.

(7) Stankovich, S.; Dikin, D. A.; Dommett, G. H. B.; Kohlhaas, K. M.; Zimney, E. J.; Stach, E. A.; Piner, R. D.; Nguyen, S.-B. T.; Ruoff, R. S. Graphene-Based Composite Materials. *Nature* **2006**, *442*, 282−286.

(8) Tsoukleri, G.; Parthenios, J.; Papagelis, K.; Jalil, R.; Ferrari, A. C.; Geim, A. K.; Novoselov, K. S.; Galiotis, C. Subjecting a Graphene Monolayer to Tension and Compression. *Small* **2009**, *5*, 2397−2402.

(9) Poot, M.; van der Zant, H. S. J. Nanomechanical Properties of Few-Layer Graphene Membranes. *Appl. Phys. Lett.* **2008**, *92*, 063111.

(10) Lee, C.; Wei, X.; Kysar, J. W.; Hone, J. Measurement of the Elastic Properties and Intrinsic Strength of Monolayer Graphene. *Science* **2008**, *321*, 385−388.
(11) Lindahl, N.; Midtvedt, D.; Svensson, J.; Nerushev, O. A.; Lindvall, N.; Isacsson, A.; Campbell, E. E. B. Determination of the Bending Rigidity of Graphene via Electrostatic Actuation of Buckled Membranes. *Nano Lett.* **2012**, *12*, 3526−3531.
(12) Politano, A.; Marino, A. R.; Campi, D.; Farias, D.; Mirand, R.; Chiarello, G. Elastic Properties of a Macroscopic Graphene Sample from Phonon Dispersion Measurements. *Carbon* **2012**, *50*, 4903−4910.
(13) Liu, X.; Robinson, J. T.; Wei, Z.; Sheehan, P. E.; Houston, B. H.; Snow, E. S. Low Temperature Elastic Properties of Chemically Reduced and CVD-Grown Graphene Thin Films. *Diamond Relat. Mater.* **2010**, *19*, 875−878.
(14) Liu, X.; Metcalf, T. H.; Robinson, J. T.; Houston, B. H.; Scarpa, F. Shear Modulus of Monolayer Graphene Prepared by Chemical Vapor Deposition. *Nano Lett.* **2012**, *12*, 1013−1017.
(15) Hod, O.; Scuseria, G. Electromechanical Properties of Suspended Graphene Nanoribbons. *Nano Lett.* **2009**, *9*, 2619−2622.
(16) Zhao, H.; Min, K.; Aluru, N. R. Size and Chirality Dependent Elastic Properties of Graphene Nanoribbons under Uniaxial Tension. *Nano Lett.* **2009**, *9*, 3012−3015.
(17) Poetschke, M.; Rocha, C. G.; Foa Torres, L. E. F.; Roche, S.; Cuniberti, G. Modeling Graphene-Based Nanoelectromechanical Devices. *Phys. Rev. B* **2010**, *81*, 193404.
(18) Hajgato, B.; Guryel, S.; Dauphin, Y.; Blairon, J. M.; Miltner, H. E.; van Lier, G.; de Proft, F.; Geerlings, P. Theoretical Investigation of the Intrinsic Mechanical Properties of Single- and Double-Layer Graphene. *J. Phys. Chem. C* **2012**, *116*, 22608−22618.
(19) Wei, Y.; Wang, B.; Wu, J.; Yang, R.; Dunn, M. L. Bending Rigidity and Gaussian Bending Stiffness of Single-Layered Graphene. *Nano Lett.* **2013**, *13*, 26−30.
(20) Zhang, D.-B.; Akatyeva, E.; Dumitrică, T. Bending Ultrathin Graphene at the Margins of Continuum Mechanics. *Phys. Rev. Lett.* **2011**, *106*, 255503.
(21) Tapasztó, L.; Dumitrică, T.; Kim, S. J.; Nemes-Incze, P.; Hwang, C.; Biró, L. P. Breakdown of Continuum Mechanics for Nanometre-Wavelength Rippling of Graphene. *Nat. Phys.* **2012**, *8*, 739−742.
(22) Nikiforov, I.; Tang, D.-M.; Wei, X.; Dumitrică, T.; Golberg, D. Nanoscale Bending of Multilayered Boron Nitride and Graphene Ribbons: Experiment and Objective Molecular Dynamics Calculations. *Phys. Rev. Lett.* **2012**, *109*, 025504.
(23) Dumitrică, T.; James, R. D. Objective Molecular Dynamics. *J. Mech. Phys. Solids* **2007**, *55*, 2206−2236.
(24) Zhang, D.-B.; Hua, M.; Dumitrică, T. Stability of Polycrystalline and Wurtzite Si Nanowires via Symmetry-Adapted Tight-Binding Objective Molecular Dynamics. *J. Chem. Phys.* **2008**, *128*, 084104.
(25) Rurali, R.; Hernandez, E. H.; Trocadero, A. Multiple-Algorithm Multiple-Model Atomistic Simulation Program. *Comput. Mater. Sci.* **2003**, *28*, 85−106.
(26) Porezag, D.; Frauenheim, Th.; Kohler, Th.; Seifert, G.; Kaschner, R. Construction of Tight-Binding-Like Potentials on the Basis of Density-Functional Theory: Application to Carbon. *Phys. Rev. B* **1995**, *51*, 12947−12957.
(27) Carlson, A.; Dumitrică, T. Extended Tight-Binding Potential for Modeling Intertube Interactions in Carbon Nanotubes. *Nanotechnology* **2007**, *18*, 065706.
(28) Zhang, D.-B.; Dumitrică, T. Elasticity of Ideal Single-Walled Carbon Nanotubes via Symmetry-Adapted Tight-Binding Objective Modeling. *Appl. Phys. Lett.* **2008**, *93*, 031919.
(29) Zhang, D.-B.; James, R. D.; Dumitrică, T. Electromechanical Characterization of Carbon Nanotubes in Torsion via Symmetry-Adapted Tight-Binding Objective Molecular Dynamics. *Phys. Rev. B* **2009**, *80*, 115418.
(30) James, R. D. Objective Structures. *J. Mech. Phys. Solids* **2006**, *54*, 2354−2390.
(31) Timoshenko, S. P.; Gere, J. M. *Theory of Elastic Stability*, 2nd ed.; McGraw-Hill: New York, 1961.
(32) Torsion experiments on metal wires revealed lengthening of wires, a behavior known as the Poynting effect. See: Poynting, J. H. On Pressure Perpendicular to the Shear Planes in Finite Pure Shears, And on the Lengthening of Loaded Wires When Twisted. *Proc. R. Soc. London, Ser. A* **1909**, *82*, 546−559.
(33) The microscopic shear strain was calculated by measuring the angle change between neighboring bonds. The value plotted in Figure 2c is an average over all bonds within the ribbon.
(34) Zhang, D.-B.; Dumitrică, T. Effective Tensional-Strain Driven Band-Gap Modulations in Helical Graphene Nanoribbons. *Small* **2011**, *7*, 1023−1027.
(35) Zhang, D.-B.; Dumitrică, T. Role of the Effective Tensile Strain in the Electromechanical Response of Helical Graphene Nanoribbons with Open and Closed Edges. *Phys. Rev. B* **2012**, *85*, 035445.